

Tunneling Splittings in the S_0 and S_1 States of the Benzoic Acid Dimer Determined by High-Resolution UV Spectroscopy

Ivo Kalkman,^[a] Chau Vu,^[b] Michael Schmitt,^{*[b]} and W. Leo Meerts^{*[a]}

Five different isotopologues of the benzoic acid dimer and a vibronic band located 57 cm^{-1} above the electronic origin, which is assigned to the out-of-plane butterfly motion, are studied by rotationally resolved UV spectroscopy. From these measurements a ground-state structure with C_{2h} symmetry is deduced, whereas the symmetry is lowered to C_s in the S_1 state. The increase in the

center-of-mass distance between the two monomers that is found on electronic excitation indicates a decrease in hydrogen-bond strength. The tunneling splittings in the S_0 and S_1 states are 1385.2 ± 0.7 and 271.2 ± 0.7 MHz, respectively, corresponding to an increase in barrier height by 7.2% on electronic excitation.

1. Introduction

Hydrogen bonding is very important in biological systems and has therefore been the subject of considerable research. Some systems employ multiple hydrogen bonds to connect molecular subunits; most notable among these is DNA, the base pairs of which are connected by double or triple hydrogen bonds. Because of their high symmetry, the dimers of carboxylic acids such as formic acid, acetic acid, and benzoic acid have become model systems for double hydrogen bonding. Their carboxyl groups link to create an eight-membered ring and, in the above examples, a ground-state dimer structure of C_{2h} symmetry. This doubly hydrogen-bonded structure is so strong that even at room temperature mostly dimers are present.

Since many biologically relevant processes involve proton transfer, an interesting aspect of carboxylic acid dimers is the possibility of double proton tunneling. The tunneling path has long been the subject of debate, however, and theoretical estimates of proton transfer times span several orders of magnitude (e.g., see Madeja and Havenith^[1] and references therein). Early calculations agreed that extensive geometry optimization of the transition state is necessary and that the transition itself is strongly coupled to a deformation of the whole molecular frame, but the predicted barrier heights differed significantly.^[2,3] Anomalous isotope effects observed for two vibrations of formic acid dimer led Maréchal to conclude that the transfer of protons can not be described as a simple tunneling motion in a double-minimum potential.^[4] Recent direct dynamics calculations with a single multidimensional coordinate system could explain a variety of gas-phase and crystal data by carefully considering the contributions of various zero-point vibrations to the tunneling rates and assuming a negligible splitting in the electronically excited state.^[5] Coupling between the tunneling mode and transverse modes was calculated to result in a more than 20-fold increase in the tunneling splitting. Recently, ^1H NMR relaxometry and quasi-elastic neutron scattering have shown conclusively that proton transfer in the benzoic acid crystal is a strongly correlated motion of the two protons,

while the tunneling path is little affected by deuteration in the carboxyl group.^[6] Fillaux et al. deduced from spectra of powdered crystals that the potential barrier for the transfer of a single proton is already on the order of 5000 cm^{-1} , which means that semiclassical jumping over the top is negligible.^[7] In conclusion, the picture that has emerged is that double proton transfer in carboxylic acid dimers is a pure tunneling motion that occurs in concert, initiated by a zero-point vibrationally induced symmetric decrease of the distance between the two monomer units.

Experimental data on the barriers for concerted proton tunneling reflect the sensitive dependence on the vibrations in both monomer units. In one of the earliest measurements on such systems, Costain and Srivastava found that the barrier height is larger than 6000 cm^{-1} in $\text{CF}_3\text{COOH}\cdots\text{HCOOH}$, but less than 5000 cm^{-1} in $\text{CF}_3\text{COOH}\cdots\text{CH}_3\text{COOH}$.^[8] From fluid-phase absorption spectra the barrier heights in dimers of formic acid and acetic acid were deduced to be in the range $6500\text{--}7000\text{ cm}^{-1}$ when a symmetric double-minimum potential is assumed.^[9] By means of high-resolution gas-phase IR spectroscopy on various isotopologues of the formic acid dimer, ground-state tunneling splittings of 375 and 474 MHz were observed

[a] I. Kalkman, Prof. W. L. Meerts
Molecular and Biophysics Group
Institute for Molecules and Materials, Radboud University Nijmegen
P.O. Box 9010, 6500 GL Nijmegen (The Netherlands)
Fax: (+31) 24-365-33-11
E-mail: Leo.Meerts@science.ru.nl

[b] C. Vu, Dr. M. Schmitt
Institut für Physikalische Chemie und Elektrochemie I
Mathematisch-Naturwissenschaftliche Fakultät
Heinrich-Heine-Universität Düsseldorf
Universitätsstraße 26.43.02.43, 40225 Düsseldorf (Germany)
Fax: (+49) 211-81-15195
E-mail: Mschmitt@uni-duesseldorf.de

Supporting information for this article is available on the WWW under <http://dx.doi.org/10.1002/cphc.200800214>.

for the (DCOOH)₂ and (HCOOH)₂ dimers, respectively, whereas for the (DCOOD)₂ dimer an upper limit of 60 MHz was deduced.^[1,10,11] This corresponds well with an effective barrier height of 6940 cm⁻¹ for the fully protonated dimer.^[5]

Attempts to determine the magnitude of the tunneling splitting in the benzoic acid dimer have mainly been made by using crystallographic methods. Although the crystal of benzoic acid is composed of dimeric units, its lattice structure destroys the symmetry between the two monomers, and this results in two inequivalent potential minima and an inability to determine the tunneling splitting. However, with a suitable dopant the inequivalence between the two minima can be nearly lifted locally to allow a coarse estimate. The values found with thioindigo and selenoindigo as dopants were 8.4 ± 0.1 and 6.5 ± 1.5 GHz, respectively.^[12,13] Remmers et al.^[14] studied the gas-phase dimer using high-resolution UV spectroscopy. The spectrum they recorded consisted of two rigid-rotor components separated by 1107 ± 7 MHz, which they assumed to be the difference between the tunneling splittings in the S₀ and S₁ states. These data were later re-analyzed by using genetic algorithms to yield a more accurate value of 1116 ± 3 MHz.^[15] Smedarchina et al. theoretically reproduced this value quite well (1920 MHz) by assuming that it was due solely to the ground-state splitting, taking it to be zero in the excited state, and showed that it corresponds to an effective tunneling barrier of 5793 cm⁻¹.^[5]

Electronic coupling between the two monomer units in a doubly hydrogen-bonded system depends very sensitively on the nature of the hydrogen bonds. Perhaps the most striking example of this is the 7-azaindole dimer, in which electronic excitation was shown to be localized on one of the monomer units in all isotopologues, with the exception of a single asymmetric, doubly deuterated structure, in which it was found to be completely delocalized.^[16,17] This is remarkable, since the last-named structure only differs from two others by monodeuteration in the aromatic ring. Fortunately, in many other systems the situation seems to be more clear-cut. In the 2-pyridone dimer the excitation is completely delocalized,^[18,19] whereas in carboxylic acids the excitation generally seems to be localized.^[20–22] By observing a vibronic band in the gas-phase benzoic acid dimer split into four components on partial deuteration, Poeltl et al. showed that also in this system electronic excitation resides on a single half of the complex.^[23,24]

Localization of excitation raises the question how feasible excitation transfer is. Very interesting in this respect is the existence of a vibronic band around 57 cm⁻¹ above the origin of the benzoic acid dimer. This band is shared with many other carboxylic acid dimers, including that of anthranilic acid, for which it was recently found that, although there is a strong Franck–Condon progression in this mode, the dispersed fluorescence spectrum shows intensity only in even members of the progression.^[20] By means of DFT calculations, the band was assigned as the intermolecular geared bend mode, and the anomalous intensity patterns were explained by the possibility of excitation transfer between the two monomers, altering the selection rules.^[25] Due to large intramolecular geometry changes on excitation of a monomer unit, however, the exci-

ton splitting could not be observed directly. The corresponding vibronic band of the benzoic acid dimer shows the same anomalous intensity pattern, but a detailed analysis of intramolecular vibrational relaxation (IVR) rates in isotopically mixed dimers led to the conclusion that excitation transfer is only appreciable at higher excess energies.^[24] Still, due to the absence of an intramolecular hydrogen bond, the intramolecular geometry changes on electronic excitation are much smaller in the benzoic acid dimer than in the anthranilic acid dimer, which means an exciton splitting might be observable in the vibronic band of benzoic acid dimer. This was also suggested by Baum et al., though given their upper limit of 0.3 cm⁻¹, such a measurement would require high resolution.^[26]

The assignment of this band is the topic of some debate. Poeltl et al. initially suggested it to be the intermolecular geared bend mode. This was because it forms strong combination bands with other vibrations ascribed to internal motions in the carboxyl group, and due to the observation that in the completely ring-deuterated (d₅-d₅) dimer the vibrational frequency remains virtually unchanged.^[23] They later favored reassignment as either the out-of-plane bending motion or torsion, given that its frequency is unchanged in the electronically excited state.^[24] Dispersed fluorescence spectra of this band led Tomioka et al. to assume that it is the torsion mode.^[27] Quantum chemical calculations seem to disagree among each other to the same extent. Based on DFT calculations, Nandi et al. assigned it as the geared bend motion,^[28] while Antony et al. claimed that it is the torsion mode,^[29] and according to Florio et al. it could be either the geared bend or tilting motion.^[30,31] Bakker et al. found that the difficulties in accurately describing the hydrogen-bonded modes also play a role in the calculation of higher vibrations (500–1900 cm⁻¹).^[32]

Herein, we determine the intermolecular structure in both the ground and electronically excited state from seven different dimer origins in high-resolution spectra. Of particular interest is the question whether a decrease in the carboxyl O...O distance can be observed, as has been suggested,^[8,11] and whether the excited state has a bent structure, as was proposed earlier.^[14] Furthermore, analysis of a high-resolution spectrum of the 57 cm⁻¹ vibronic band should show whether exciton splitting is present and which vibration is involved. Lastly, this assignment should allow us to determine the splittings of the S₀ and S₁ states separately, as well as the relative tunneling barrier height.

Experimental Section

Experimental Procedures: The experimental setup for rotationally resolved laser-induced fluorescence (LIF) is described elsewhere.^[33] Briefly, it consists of a ring dye laser (Coherent 899-21) containing Rhodamine 110, pumped with 6 W of a frequency-doubled Yb:YAG laser. The second harmonic of the dye-laser output is generated in an external folded ring cavity (Spectra Physics Wavetrain). The resulting output power is typically between 30 and 40 mW and is constant during each experiment. The molecular beam is formed by co-expanding benzoic acid, heated to 390 K, and argon through a 100 μm nozzle into the vacuum by using a backing pressure of 220 mbar. The molecular-beam equipment consists of three differ-

entially pumped vacuum chambers that are linearly connected by skimmers (1 and 3 mm in diameter, respectively) in order to reduce the Doppler width. In the third chamber, 360 mm downstream of the nozzle, the molecular beam is crossed at right angles by the UV laser beam. Imaging optics focus the total undispersed fluorescence from the excited molecules onto a photomultiplier tube mounted perpendicularly to the plane defined by the laser and the molecular beam, the output of which is then discriminated and digitized by a photon counter and transmitted to a PC for data recording and processing. The resulting Doppler width in this setup is 25 MHz (FWHM). Relative frequencies are determined with a quasi-confocal Fabry–Perot interferometer with a free spectral range (FSR) of 149.9434(56) MHz. The absolute frequency was obtained by comparing the recorded absorption spectrum of iodine with tabulated lines.^[34]

Materials: Benzoic acid was purchased from Caelo (p.A.), and [D₂]benzoic acid (99.2%) was obtained from CDN isotopes. Both were used without further purification. [D₁]Benzoic acid was produced by refluxing benzoic acid with an excess of D₂O and subsequent removal of the solvent.

Ab Initio Calculations: Structure optimizations were performed by employing the valence triple-zeta basis set with one set of polarization functions per atom (TZVP) from the TURBOMOLE library.^[35,36] The equilibrium geometries of the electronic ground and the lowest excited singlet states were preoptimized by (time-dependent) density functional theory with the B3LYP functional and subsequently optimized at the CC2 level within the resolution-of-the-identity approximation.^[37,38] To ensure that the optimized structure is a real minimum we numerically calculated the second derivatives. We obtained no imaginary frequencies for any of the normal modes, that is, all optimized structures are minima.

The singlet-state energies and wavefunctions were calculated by the combined DFT/multireference configuration interaction (DFT/MRCI) method of Grimme and Waletzke.^[39] The configuration state functions in the MRCI expansion are constructed from Kohn–Sham (KS) orbitals, optimized for the dominant closed-shell determinant of the electronic ground state by employing the BHLYP^[40,41] functional. All valence electrons were correlated in the MRCI runs, and the eigenvalues and eigenvectors of eight singlet states were determined. The initial set of reference configuration state functions was generated automatically in a complete active-space-type procedure (including all single and double excitations from the five highest occupied molecular orbitals in the KS determinant to the five lowest virtual orbitals) and was then iteratively improved.

The first-order transition state for double proton transfer was pre-optimized at the B3LYP level with the 6-31G(d,p) basis set by using the QST3 method^[42] as implemented in the Gaussian03 program package.^[43] With the thus-obtained structure the S₀ transition state was optimized at the RICC2 level by using the trust radius image minimization (TRIM) method^[44] implemented in the STATPT module from TURBOMOLE V5.8 with the same basis sets as for the minimum structures.

The Derandomized ES DR2 Algorithm: Spectra were fitted to a simple asymmetric rotor Hamiltonian by using a derandomized (DR) evolutionary strategy (ES) which was developed in the mid-90s by Ostenmeier et al.^[45] This special implementation, which is also used herein, represents the second generation of derandomized ES and is abbreviated in the following as DR2.^[46] It is shown here to be a very good alternative to the genetic algorithm based fits we have employed so far.^[47,48]

Both evolutionary strategies like the DR2 algorithm and the genetic algorithm belong to the category of global optimizers known as evolutionary algorithms, which were inspired by the biological processes of reproduction and natural selection. However, whereas the genetic algorithm tries to find a solution in parameter space by combining information from a set of trial solutions with the aim of creating better ones, the DR2 algorithm can sense in which direction the fitness increases. In a first step of the DR2 algorithm, some trial solutions are generated (offspring) by using a random distribution around some starting point (parent), each consisting of the complete parameter set necessary to describe the spectrum, and the quality of each solution is analyzed by means of a fitness function.^[47,48] Provided one of the offspring is better than the parent, this solution is selected and used to compute the next parent, which then serves as the starting point for an iteration of this cycle (generation). In calculating the parent for the next generation, the DR2 algorithm makes use of the correlation matrix for successive changes in the parents (mutations). In essence, this means that if for some parameter a parent has evolved in the same direction for several generations, so that their correlation in this parameter is positive, the most likely solution is assumed to be further in that direction and the next parameter mutation will be larger. Correspondingly, two anticorrelated mutations will lead to a smaller mutation. By discriminating between mutation rates of different parameters, the DR2 algorithm can reliably find the optimal solution within a relatively small number of generations.^[45]

The usefulness of the DR2 algorithm in solving physical problems was shown by Shir et al., who tested several evolutionary algorithms for their ability to find the theoretical alignment of a sample of molecules in space with shaped laser pulses.^[49] The DR2 algorithm proved to be not only the fastest but also the most reliable algorithm for this task, and it even outperformed several more advanced algorithms such as DR3 and CMA–ES. Given their success they then turned their attention to the problem of second harmonic generation (SHG) which, although much more difficult, showed that the DR2 algorithm again performed best.^[46] When used to fit our spectra, the DR2 algorithm succeeded in obtaining good fits with a smaller population and within fewer generations compared to the genetic algorithm (GA). Although the evaluation of a single trial solution in the DR2 algorithm is more expensive, this led to a reduction in the total computation time by a factor of two compared to the GA.

2. Results and Discussion

2.1. The Dimer Origin

The rotationally resolved spectrum of the S₁←S₀ origin of the benzoic acid dimer has been reported before,^[14,15] but was measured again for this study. It is a b-type spectrum and shows doubling of all lines due to concerted proton tunneling in the double hydrogen bond. The size of this splitting is $\Delta = 1114.0 \pm 1.0$ MHz. The spectrum is very congested, and each apparent transition typically consists of some ten individual rovibrational transitions. The transitions in these *K* stacks all share the same ΔK_v , but differ in the ground-state level from which they originate. Under our experimental conditions, transitions originating from ground-state levels with *J* values up to 130 are needed to reproduce contributions to the spectrum with an intensity of at least 0.5% of the strongest transitions. Since there is no thermal equilibrium in the molecular beam,

we employ a two-temperature Boltzmann model to describe the energy distribution. This resulted in rotational temperatures of $T_1=3.5$ K and $T_2=5.3$ K with a relative T_2 weight factor of 0.29.

Besides the d_0-d_0 dimer we measure the $S_1 \leftarrow S_0$ origin of four more isotopologues, which give rise to six additional spectra. These are the d_1-d_1 and d_5-d_5 homodimers, where the former is deuterated in the hydrogen bonds and the rings of the latter are completely deuterated, and the $d_0^*-d_1/d_1^*-d_0$ and $d_0^*-d_5/d_5^*-d_0$ mixed dimers. Here the asterisk denotes the electronically excited moiety. Due to the weak electronic coupling between the two monomer units, the electronic excitation is localized on one of them, and as a result both mixed dimers have two separate origins depending on which monomer is excited.^[23] However, since the isotopic shifts upon deuteration are small, the origins of these mixed dimers (with the exception of the $d_5^*-d_0$) are not spectrally separated from the homodimers consisting of the excited monomer and have therefore not been resolved in previous studies. As an example the spectrum of the $d_0^*-d_5$ dimer is shown in Figure 1 together with a simulated spectrum. The simulation consists of two components: the spectrum of d_0-d_0 , for the simulation of which the molecular constants are held fixed to the optimal values determined there, and the spectrum of $d_0^*-d_5$ itself, blueshifted by 0.67 cm^{-1} . All other spectra and their simulations can be found in the Supporting Information.

Within the experimental uncertainty all initial simulations produce transition dipole moment directions corresponding to pure b-type spectra, and no a-type or c-type components can be incorporated unambiguously. Therefore, to obtain the final results a pure b-type asymmetric rotor Hamiltonian is used. Also, for $d_0^*-d_1$ and $d_1^*-d_0$ as well as $d_0^*-d_5$ and $d_5^*-d_0$, the

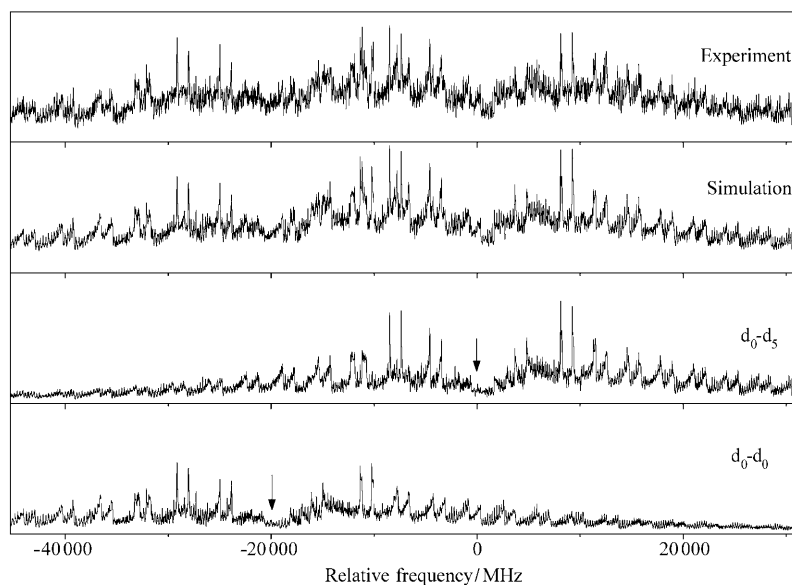


Figure 1. Electronic origin of the benzoic acid $d_0^*-d_5$ dimer at 35724.456 cm^{-1} . In the upper two traces the measured spectrum and the best simulation are shown. The lower two traces show the two components present in the simulation, that is, the $d_0^*-d_5$ spectrum and the d_0-d_0 spectrum, for the latter of which the molecular parameters deduced from the analysis of a separate measurement were used. The arrows indicate the spectral origins.

ground-state rotational constants for each set are the same within their experimental uncertainties, that is, both spectra in each of these two sets indeed originate from a common ground state structure. In a final fit the ground-state rotational constants for both spectra in each set are therefore forced to be equal. The parameters obtained from the final fits are given

Table 1. Origins and molecular parameters for the isotopologues of the benzoic acid dimer determined from fits using evolutionary algorithms.

	This work	d_0-d_0 Ref. [14]	Ref. [15]	d_0-d_0+57 cm^{-1}	d_1-d_1	d_5-d_5
A' [MHz]	1925.00(20)	1923(16)	1926.87(50)	1925.04(21)	1905.94(18)	1686.92(16)
B' [MHz]	128.05(14)	127(8)	128.19(10)	128.08(14)	127.73(14)	118.91(14)
C' [MHz]	120.14(14)	114(8)	120.27(10)	120.17(14)	119.79(14)	111.16(14)
A'' [MHz]	1908.95(16)	1908(16)	1910.70(50)	1920.48(17)	1890.16(15)	1672.95(13)
B'' [MHz]	127.53(14)	–	127.67(10)	127.57(14)	127.18(14)	118.42(14)
C'' [MHz]	119.63(14)	–	119.76(10)	119.64(14)	119.24(14)	110.68(14)
ΔA [MHz]	–16.05(9)	–15(10)	–16.17(20)	–4.56(9)	–15.78(8)	–13.98(7)
ΔB [MHz]	–0.52(12)	–	–0.52(1)	–0.52(12)	–0.55(12)	–0.48(12)
ΔC [MHz]	–0.51(12)	–	–0.51(1)	–0.53(12)	–0.55(12)	–0.48(12)
Δ [MHz]	1114.0(10)	1107(7)	1116(3)	1656.4(11)	< 45	1077.0(10)
Origin [cm^{-1}] ^[a]	35723.786(1)	35723.82(5)	–	35781.091(1)	35737.416(1)	35874.324(1)
	$d_0^*-d_1$		$d_1^*-d_0$	$d_0^*-d_5$		$d_5^*-d_0$
A' [MHz]	1915.76(32)		1915.76(17)	1798.21(14)		1798.21(15)
B' [MHz]	127.91(15)		127.91(14)	123.42(14)		123.42(14)
C' [MHz]	119.98(15)		119.98(14)	115.58(14)		115.58(14)
A'' [MHz]	1899.65(26)		1900.51(14)	1784.55(12)		1782.50(12)
B'' [MHz]	127.39(15)		127.33(14)	122.95(14)		122.90(14)
C'' [MHz]	119.50(15)		119.42(14)	115.11(14)		115.07(14)
ΔA [MHz]	–16.11(16)		–15.25(10)	–13.66(6)		–15.72(7)
ΔB [MHz]	–0.50(12)		–0.57(12)	–0.46(12)		–0.52(12)
ΔC [MHz]	–0.50(12)		–0.56(12)	–0.48(12)		–0.51(12)
Δ [MHz]	136.7(12)		98.9(11)	1137.0(10)		1116.9(11)
Origin [cm^{-1}] ^[a]	35722.789(1)		35737.574(1)	35724.456(1)		35872.481(1)

[a] In the spectra with splitting, the origin of the reddest component is given.

in Table 1. The estimated lifetime broadening of the transitions is 20 ± 10 MHz, corresponding to an excited state lifetime of 8 ± 4 ns. Unfortunately, the congested nature of the spectra prohibits a more accurate determination.

Immediately obvious is that the changes in the rotational constants (ΔB_g ; $g = a, b, c$) are largely independent of deuteration, and thus the spectra are qualitatively very similar in appearance. Strikingly, both for the $d_0^* - d_1/d_1^* - d_0$ and the $d_0^* - d_2/d_2^* - d_0$ mixed dimers, the two spectra originating from the same ground state show substantially different tunneling splittings. In the case of $d_1 - d_1$, no splitting is observed. From test calculations we estimate how large the separation between two closely spaced spectral components must be in order to observe both. This results in a value of 45 MHz, which indicates an upper value for the splitting.

2.2. The 57 cm^{-1} Vibronic Band

Figure 2 shows the rotationally resolved spectrum of the vibronic band located 57 cm^{-1} above the electronic origin of the $d_0 - d_0$ dimer. Although the signal-to-noise ratio is more than an order of magnitude lower than that of the origin spectrum, the agreement between simulation and experiment is clearly still very good. On comparison with the origin spectrum it is also apparent that the amount by which all lines are split due to tunneling is substantially larger; the fit yields a value of 1656.4 ± 1.1 MHz, which corresponds to an increase of almost 50%. The molecular parameters resulting from this fit are listed in Table 1.

2.3. Determination of the Cluster Structure Parameters

The RICC2 optimizations of the S_0 state structure with imposed C_1 and C_{2h} symmetry restrictions are performed with the TZVP basis sets. The results of both calculations are identical within

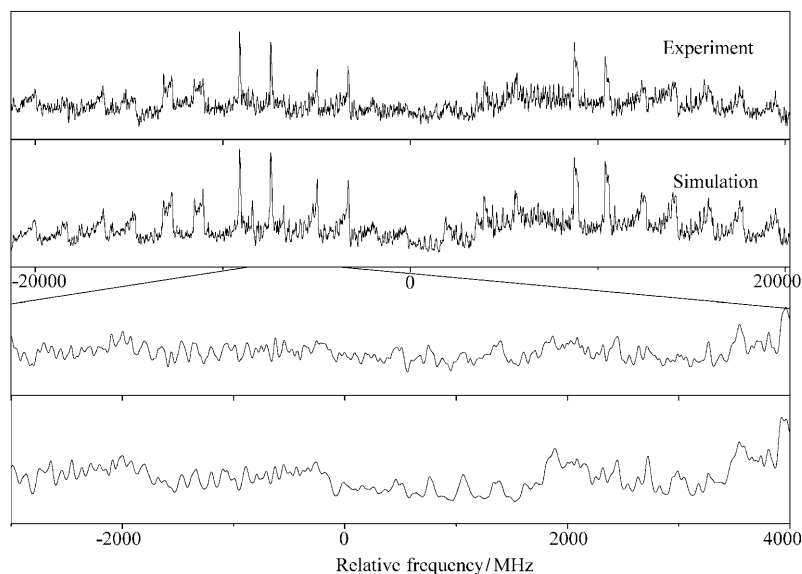


Figure 2. Vibronic band at $35781.091 \text{ cm}^{-1}$, around 57 cm^{-1} above the electronic origin of the benzoic acid $d_0 - d_0$ dimer.

the accuracy of the calculation, and this confirms the symmetry of the equilibrium structure. The rotational constants resulting from the constrained calculations are listed in Table 2 along with the experimental rotational constants from this study and the optimized geometric parameters. The agreement between calculated and experimental inertial parameters is very good, with the calculated constants differing from the measured ones by less than half a percent. Since the experimentally determined rotational constants are effective values rather than equilibrium values, we ascribe the difference to effects of zero-point energy vibrational averaging and assume the calculated structure to be the best possible fit to our measurements. The S_1 state optimizations at the same level of theory result in rotational constants close to those of the ground state. The A constant is found to decrease by 16 MHz on electronic excitation, which compares to a difference of 19 MHz between the RICC2/TZVP calculations of the excited state and the electronic ground state.

The atomic numbering of the benzoic acid dimer used in the discussion of the structural parameters of the monomers and the hydrogen-bond parameters is shown in Figure 3. The

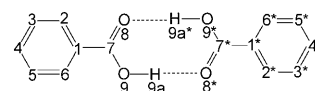


Figure 3. Atomic numbering of the benzoic acid dimer used in Table 2. The asterisks mark the electronically excited benzoic acid moiety.

calculated geometric parameters for both benzoic acid moieties are equal for the ground state (C_{2h} symmetry), while they differ considerably for the electronically excited state, reflecting the localized excitation with a reduction of the symmetry to C_s . The electronically excited benzoic acid moiety (marked with asterisks in the bond definitions in Table 2) shows an increase of the average C–C bond length from 139.4 pm in the ground state to 143.0 pm, which is typical for benzenoid aromatic compounds. The unexcited moiety of the electronically excited dimer has an average C–C bond length of 139.6 pm, which is nearly the same as in the ground state and confirms localization of excitation on one of the benzoic acid moieties. The decrease of the C1–C7 bond length, indicating quinoidal character in the S_1 state, is also found in other monosubstituted benzenes.

The hydrogen-bond geometric parameters show the same behavior: two equal O9–H9a bond lengths and equal O9–H9a–O8* angles, which define

the deviation from linearity of the hydrogen bonds in the electronic ground state, while both geometric parameters differ considerably in the excited state. The COH...OC* hydrogen bond is considerably shorter than in the electronic ground state (-5.2 pm), while the *COH...OC bond is longer by 1.8 pm. These opposite changes of the hydrogen-bond lengths, which are founded in the decreased OH acidity on electronic excitation, result in in-plane tilting of the monomer moieties in the excited state. The amount by which the structure is bent cannot be determined in the same way as was done by Remmers et al.,^[14] since they assumed both monomer geometries were retained in the dimer, which is not the case and leaves their bending angle ill-defined. When we instead define the bending angle as C4-CM-C4*, where CM stands for the center of mass of the dimer, a value of $0.7 \pm 0.2^\circ$ results. Since the decrease in length of the shortened hydrogen bond is larger than the increase in length of the elongated one, these results are consistent with the reduction in the average carboxyl O...O distance found in earlier work.^[8,11]

2.4. Determination of the Center-of-Mass Distance

An easy approach to the change of the cluster structure upon electronic excitation can be made by using the center-of-mass (COM) distance of the monomer moieties in the cluster, as has been shown by Connell et al.^[50] The COM distance of two monomer moieties in a dimer is given by Equation (1)

$$R = \sqrt{\frac{\sum_g I_g^{\text{Dimer}} - \sum_g I_g^{\text{Monomer1}} - \sum_g I_g^{\text{Monomer2}}}{2\mu}} \quad (1)$$

where μ is the reduced mass of the two moieties, and I_g are the respective moments of inertia, described by their superscripts, which are calculated from experimentally determined rotational constants. The COM distances for d_0-d_0 and d_1-d_1 in

Table 2. Rotational constants and S_0 - and S_1 -state geometric parameters of the benzoic acid dimer calculated at the RICC2/TZVP level of theory. The atomic numbering refers to Figure 3. All bond lengths are given in picometers, and angles in degrees. Atoms marked with an asterisk belong to the electronically excited benzoic acid moiety.

	S_0			S_1	
	RICC2	Crystal data ^[53]	Exptl. ^[a]	RICC2	Exptl. ^[a]
A'' [MHz]	1919	–	1925	1900	1909
B'' [MHz]	128	–	128	127	127
C'' [MHz]	120	–	120	119	120
C1–C2	139.9	139.2	–	140.0	–
C2–C3	139.2	140.1	–	139.3	–
C3–C4	139.5	138.4	–	139.6	–
C4–C5	139.6	137.9	–	139.6	–
C5–C6	139.1	138.7	–	139.2	–
C6–C1	139.9	139.0	–	140.0	–
C1–C7	148.3	148.4	–	148.6	–
C7–O8	124.0	126.3	–	124.2	–
C7–O9	130.0	127.5	–	132.8	–
O9–H9a	100.3	ca. 100	–	100.2	–
C–H (av)	108.3	–	–	108.4	–
C2–C1–C7	121.3	118.8	–	121.3	–
O8–C7–O9	123.8	123.2	–	124.0	–
C1–C7–O8	122.2	120.2	–	121.9	–
C7–O9–H9a	108.5	–	–	108.8	–
C1*–C2*	139.9	139.2	–	143.4	–
C2*–C3*	139.2	140.1	–	143.2	–
C3*–C4*	139.5	138.4	–	141.9	–
C4*–C5*	139.6	137.9	–	142.9	–
C5*–C6*	139.1	138.7	–	143.1	–
C6*–C1*	139.9	139.0	–	143.4	–
C1*–C7*	148.3	148.4	–	144.3	–
C7*–O8*	124.0	126.3	–	125.7	–
C7*–O9*	130.0	133.1	–	134.5	–
O9*–H9a*	100.3	ca. 100	–	100.0	–
C*–H* (av)	108.3	–	–	108.3	–
C2*–C1*–C7*	121.3	118.8	–	122.8	–
O8*–C7*–O9*	123.8	123.2	–	123.6	–
C1*–C7*–O1*	122.2	120.2	–	122.2	–
C7*–O9*–H9a*	108.5	–	–	108.2	–
H9a–O8*	165.4	ca. 160	–	160.2	–
O8–H9a*	165.4	ca. 160	–	167.2	–
O8–O9*	265.7	263.3	–	267.2	–
O9–O8*	265.7	263.3	–	260.4	–
O9–H9a–O8*	179.0	–	–	177.5	–
O9*–H9a*–O8	179.0	–	–	179.1	–

[a] Experimental values from this study. For exact values and accuracies, see Table 1

the ground state were calculated by using the monomer rotational constants, taken from the microwave work of Onda et al.,^[51] for both moieties. The difference between the COM distances of d_0-d_0 and d_1-d_1 can be traced back to the different vibrational averaging in these isotopologues.

While the determination of the COM distance in the electronic ground state is conceptually easy, two problems arise for the electronically excited state: first, the rotational constants of the excited state of the monomer are not known. Second, it is not known a priori whether the excitation is local or delocalized over both moieties. In the first case different rotational constants must be used in Equation (1) for Monomer1 and Monomer2. One of the monomers would then have the

rotational constants of benzoic acid in the ground state, and the other the rotational constants of the electronically excited state. Since these rotational constants are not available, we use the ground state rotational constants of both monomers for a rough model (model 1).

Because we conclude that the electronic excitation is localized, a more accurate COM distance can be derived when the rotational constants of the monomer excited state are used. These can be obtained by calculating the structure of the benzoic acid monomer by DFT with the B3LYP functional for the ground state and with time-dependent (TD)DFT for the excited state. The difference between the two sets of rotational constants closely matches the change in the rotational constants on electronic excitation, while the absolute values are less reliable. We therefore added the difference between the calculated rotational constants from the DFT and TDDFT calculations to the microwave rotational constants to get the inertial parameters for the excited monomer moiety, and used these in a more accurate model (model 2).

Table 3 compares the COM distances in the ground and electronically excited states of the benzoic acid dimer for both monomer models. For both isotopologues and independent of the model used we find an increase in the COM distance, that is, a decrease of the hydrogen-bond strength on electronic excitation.

		d_0-d_0	d_1-d_1
S_0		712.6	708.9
S_1	model 1	714.6	713.3
S_1	model 2	713.1	711.7
Δ	model 1	2.0	4.4
Δ	model 2	0.5	2.8

2.5. Symmetry

Both the $S_1 \leftarrow S_0$ spectrum and the vibronic band 57 cm^{-1} above it are b-type spectra consisting of two components. Interestingly, the separation between these components is larger in the vibronic spectrum than in the origin spectrum. Figure 4 shows the three possible ways to combine these two observations: a) the ground-state splitting is very small, b) the S_1 -state

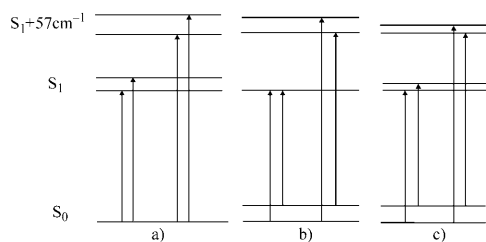


Figure 4. Three possible energy-level schemes for explaining the observed $S_1 \leftarrow S_0$ and $S_1 + 57 \text{ cm}^{-1} \leftarrow S_0$ spectra.

splitting is very small, or c) both are appreciable. Since it is expected from theory that the splitting in the electronically excited state is smaller than that in the ground state due to the weakening of one of the hydrogen bonds (e.g., see ref. [5]) we hold the first option for unlikely and will therefore not explore it further. For the other two options, some of the arrows drawn in Figure 4b and c are not unique; the relative sizes of the tunneling splittings are equally unknown. However, it is clear that without any selection rules restricting the possibilities, the vibronic band would consist of four components, and in case c the same would hold for the origin transition. This is clearly not what we observe, so a closer look at the symmetry of the dimer system is warranted. For a large part the group theory for this system is the same as for the formic acid dimer, which has been described in detail by Madeja et al.^[1] We therefore focus on the main differences and conclusions here; more information can be found in their article. Additionally, we will consider case b to be the limiting case for the energy-level ordering shown in Figure 4c and no longer consider it separately.

As shown in Section 2.3, the ground-state structure is of C_{2h} symmetry and if we assume a synchronous tunneling motion, the transition state is of D_{2h} symmetry, which means we must describe the ground state using the molecular symmetry group G_8 . For the electronically excited state, however, we already concluded that the electronic excitation is localized on one monomer unit. This immediately lowers the symmetry to C_s with a C_{2v} transition state (with the A axis as the C_2 axis) so that we must describe the excited state using G_4 . The energy-level diagram and allowed transitions that result for the origin and the seven lowest-frequency vibrations (see Section 2.6) are shown in Figure 5. Note that all levels have two symmetry labels due to the unresolved K-type doubling in this system.

If in addition to the localization of the electronic excitation the excited state has a bent structure, then the system has $C_s(M)$ symmetry (isomorphic with C_s) and all energy-level labels are transformed into A'/A'' . This means all transitions would become possible again, in contradiction with our observations.

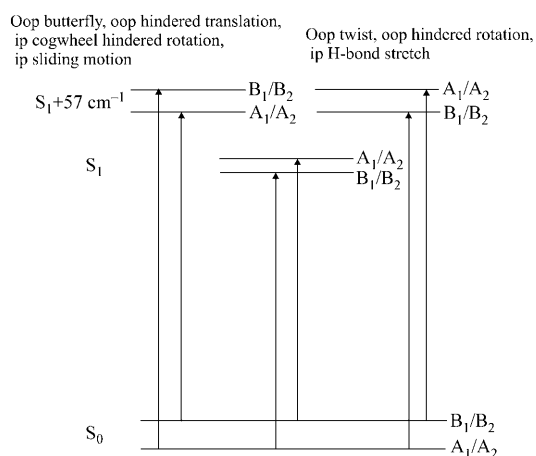


Figure 5. Energy-level ordering and allowed transitions for the electronic origin and seven lowest-frequency vibrations under C_{2v} symmetry; vibrational nomenclature after ref. [30]. Out-of-plane vibrations are designated as oop, and in-plane vibrations as ip.

Clearly the bending angle for the excited-state geometry we deduced in Section 2.3 is small enough to approximate the system as G_4 -symmetric.

The assumption of G_4 symmetry also affects the intensity ratios between different transitions. The effect, however, is small: when the K-type doubling cannot be resolved (as in our case) a ratio between $\Delta K_a \Delta K_c$ (even/even) and (even/odd) to (odd/odd) and (odd/even) transitions of 31:33 results. This effect is further diminished by the crowdedness of the spectrum, which mixes different transitions under each apparent line shape, and leads to our inability to decide on the correctness of this assumption based on nuclear statistics.

2.6. Vibronic Band Assignment

For a correct assignment of the 57 cm^{-1} band we need the calculated frequencies for the vibrations indicated in Figure 5; they are given for the S_0 state in Table 4. MOLDEN frequency files containing the optimized geometry and all intra- and intermolecular vibrations can be found in the Supporting Information.

We know from earlier work by Poeltl et al.^[24] that for this particular vibration the excited-state frequency is practically the same as that in the ground state, which allows us to use these ground-state frequencies for our assignment. They were derived under C_{2h} symmetry and the corresponding symmetry labels are given. However, as was described in Section 2.5, due to the feasibility of the tunneling motion and the localization of electronic excitation, we should use the G_4 symmetry group, which is isomorphic to C_{2v} , to describe possible transitions. For this reason G_4 symmetry labels were also added. The last three columns list the calculated changes in rotational constants for these vibrations in the harmonic approximation.

Since the splitting observed in the vibronic-band spectrum is larger than that in the origin spectrum (1656.4 vs 1114.0 MHz) it is clear that an assignment to a vibration having the same selection rules as the origin transition (those on the right-hand side in Figure 5) is only possible if the vibration itself increases the tunneling rate. Since the out-of-plane twisting motion and the out-of-plane hindered rotation leave the

hydrogen-bonding network practically unaffected, these are ruled out. The in-plane hydrogen-bond stretch is expected to increase the tunneling rate, but the motion itself would lead to a change in the B and C rotational constants. Since this contradicts our measurements, we also exclude the in-plane H-bond stretching motion as a possibility, forcing us to conclude that the selection rules for the 57 cm^{-1} vibronic band must be reversed.

Examining the four vibrations listed on the left-hand side of Figure 5, the same argument excludes the in-plane sliding motion, as it is expected to affect the B and C rotational constants as well as A , contrary to our observations. This leaves us with only three possible assignments: the out-of-plane butterfly motion, the out-of-plane hindered translation, and the in-plane cogwheel hindered rotation. Without additional information to discriminate between these modes, we opt to trust the calculated frequencies and assign the 57 cm^{-1} band as the out-of-plane butterfly motion, in excellent agreement with calculations (58 cm^{-1}). It also agrees with the observation that the frequency is virtually unchanged in the d_5 - d_5 dimer,^[23] and with the assignment made in reference [24]. Unfortunately, however, the effect of this vibration on the A rotational constant does not agree with our measurements. Indeed, even the sign of the predicted change is wrong. Although the vibrational effects on the rotational constants were calculated in the harmonic approximation and it is well-known that the vibrations in the benzoic acid dimer are highly anharmonic,^[30] we infer that this vibration must be accompanied by a structural change that is not predicted by our calculations.

2.7. Splittings

Interestingly, the out-of-plane butterfly mode involves practically no motion of the hydrogen-bonding network. If we assume that this means the effect on the tunneling rate is negligible, we can deduce the sizes of the S_0 - and S_1 -state tunneling splittings. As can be seen in Figure 5 the splitting observed in the vibronic band spectrum would then be the sum of the S_0 and S_1 tunneling splittings, whereas the separation between the two components in the origin spectrum would be equal to the difference. If we now, as in Section 2.5, take the S_0 splitting to be larger than the S_1 splitting, it immediately follows that $\Delta(S_0) = 1385.2 \pm 0.7 \text{ MHz}$ and $\Delta(S_1) = 271.2 \pm 0.7 \text{ MHz}$. In the case of a pure, coherent tunneling motion in a simple symmetric double-minimum potential well, we can now calculate the effective potential barrier V_{eff} in the WKB approximation.^[52] The imaginary frequency at the top of the barrier ω_i and the corresponding ground-state frequency ω_F were deduced from a normal-mode analysis of the S_0

Table 4. RICCS/TZVP calculated frequencies for the seven lowest S_0 state vibrations of the d_0 - d_0 and d_5 - d_5 benzoic acid dimers including their symmetry labels under the C_{2h} point group and the G_4 molecular symmetry group. Also given are the calculated changes in rotational constants to which they lead in the harmonic approximation. The MOLDEN frequency files containing the optimized geometry and all intra- and intermolecular vibrations are mandatory for the description of the vibrations. They can be found in the Supporting Information.

Vibration	Frequency [cm^{-1}]		Symmetry		$\Delta g; g = A, B, C$ [MHz]		
	d_0 - d_0	d_5 - d_5	C_{2h}	G_4	ΔA	ΔB	ΔC
Observed	57.31	–	–	–	11.49	0.00	–0.02
Oop butterfly	58.1	56.5	a_u	B_1	–14.26	–0.06	0.00
Oop hindered translation	88.6	86.7	b_g	B_1	–18.17	–0.08	0.00
Ip cogwheel hindered rotation	97.9	93.5	b_u	B_2	–8.93	–0.01	–0.05
Oop twist	110.9	101.4	a_u	A_2	–7.78	–0.03	0.00
Ip H-bond stretch	116.8	113.8	a_g	A_1	–9.57	5.40	4.69
Ip sliding motion	134.1	129.5	a_g	B_2	2.09	1.58	1.40
Oop hindered rotation	171.7	171.2	b_g	A_2	–13.33	–0.06	0.00

transition state and ground state RICC2 structures, respectively. Using the resulting values of $\omega_i = 1122 \text{ cm}^{-1}$ and $\omega_f = 3167 \text{ cm}^{-1}$ we find an S_0 -state potential barrier of 6224 cm^{-1} (7.45 kJ mol^{-1}). Because no reliable S_1 -state transition frequency was calculated, we assume the same frequencies to calculate the S_1 -state potential barrier, which results in a value of 6672 cm^{-1} (7.99 kJ mol^{-1}).

Since the approximation used here is quite crude, we do not expect these barrier heights to be very accurate, even though the S_0 -state barrier is quite close to that of 6.93 kJ mol^{-1} found in the most extensive calculation done until now.^[5] However, we do expect the ratio of the S_1 to S_0 barrier heights to be relatively accurate. Thus, we can conclude that the barrier height increases by about 7.2% on electronic excitation.

The fact that the splitting observed in the 57 cm^{-1} band spectrum can be interpreted as arising from proton tunneling while no further splitting has been observed leads to the conclusion that exciton splitting does not show up in our spectra. This leads to an upper limit of 45 MHz for the exciton splitting and confirms the conclusion from earlier work that excitation transfer only becomes important at higher excess energies.^[24]

3. Conclusions

From a measurement of the rotationally resolved spectra of five different isotopologues we observed two separate origins for each of the mixed dimers. Together with the observation that the ground-state rotational constants are the same for both of these spectra, this provides unequivocal proof that the electronic excitation is localized on one of the monomer units. From our structural analysis it can be deduced that this leads to an asymmetry in the geometry of the hydrogen-bonding network and lowering of the dimer symmetry to C_s . We also found an increase in the center-of-mass distance between the two monomer moieties, from which we conclude that the hydrogen bond is weakened upon electronic excitation. Analysis of a vibronic band located 57 cm^{-1} above the electronic origin leads us to the conclusion that it should be assigned to the out-of-plane butterfly motion and allows separate deduction of the S_0 - and S_1 -state splittings. From the resulting splittings, $\Delta(S_0) = 1385.2 \pm 0.7 \text{ MHz}$ and $\Delta(S_1) = 271.2 \pm 0.7 \text{ MHz}$, it can be concluded that the barrier height in the S_1 state is 7.2% larger than that in the S_0 state. No evidence for excitation transfer was found.

Acknowledgements

This work has been performed in the SFB 663 TP A2, Universität Düsseldorf and was printed upon its demand with financial support from the Deutsche Forschungsgemeinschaft. The authors thank the National Computer Facilities of the Netherlands Organisation of Scientific Research (NWO) for a grant on the Dutch supercomputing facility SARA. Our thanks also extend to Arno Reichelt and Christian Brand for the preparation of $[D_1]$ benzoic acid.

Keywords: benzoic acid • dimerization • hydrogen bonds • laser spectroscopy • structure elucidation

- [1] F. Madeja, M. Havenith, *J. Chem. Phys.* **2002**, *117*, 7162–7168.
- [2] F. Graf, T.-K. Ha, R. R. Ernst, *J. Chem. Phys.* **1981**, *75*, 2914–2918.
- [3] S. Nagaoka, N. Hirota, T. Matsushita, K. Nishimoto, *Chem. Phys. Lett.* **1982**, *92*, 498–502.
- [4] Y. Maréchal, *J. Chem. Phys.* **1987**, *87*, 6344–6353.
- [5] Z. Smedarchina, A. Fernández-Ramos, W. Siebrand, *J. Chem. Phys.* **2005**, *122*, 134309–134309–12.
- [6] Q. Xue, A. J. Horsewill, M. Johnson, H. Trommsdorff, *J. Chem. Phys.* **2004**, *120*, 11107–11119.
- [7] F. Fillaux, M. H. Limage, F. Romain, *Chem. Phys.* **2002**, *276*, 181–210.
- [8] C. C. Costain, G. P. Srivastava, *J. Chem. Phys.* **1964**, *41*, 1620–1627.
- [9] H. Morita, S. Nagakura, *J. Mol. Spectrosc.* **1972**, *42*, 536–546.
- [10] M. Ortlieb, M. Havenith, *J. Phys. Chem. A* **2007**, *111*, 7355–7363.
- [11] A. Gutberlet, G. W. Schwaab, M. Havenith, *Chem. Phys.* **2008**, *343*, 158–167.
- [12] A. Oppenländer, C. Rambaud, H. P. Trommsdorff, J.-C. Vial, *Phys. Rev. Lett.* **1989**, *63*, 1432–1435.
- [13] C. Rambaud, H. P. Trommsdorff, *Chem. Phys. Lett.* **1999**, *306*, 124–132.
- [14] K. Remmers, W. L. Meerts, I. Ozier, *J. Chem. Phys.* **2000**, *112*, 10890–10894.
- [15] W. L. Meerts, M. Schmitt, *Int. Rev. Phys. Chem.* **2006**, *25*, 353–406.
- [16] K. Sakota, H. Sekiya, *J. Phys. Chem. A* **2005**, *109*, 2718–2721.
- [17] K. Sakota, H. Sekiya, *J. Phys. Chem. A* **2005**, *109*, 2722–2727.
- [18] A. Held, D. W. Pratt, *J. Chem. Phys.* **1992**, *96*, 4869–4876.
- [19] A. Müller, F. Talbot, S. Leutwyler, *J. Chem. Phys.* **2002**, *116*, 2836–2847.
- [20] C. A. Southern, D. H. Levy, J. A. Stearns, G. M. Florio, A. Longarte, T. S. Zwier, *J. Phys. Chem. A* **2004**, *108*, 4599–4609.
- [21] G. Meijer, M. S. de Vries, H. E. Hunziker, H. R. Wendt, *J. Chem. Phys.* **1990**, *92*, 7625–7635.
- [22] C. K. Nandi, M. K. Hazra, T. Chakraborty, *J. Chem. Phys.* **2004**, *121*, 5261–5271.
- [23] D. E. Poeltl, J. K. McVey, *J. Chem. Phys.* **1983**, *78*, 4349–4355.
- [24] D. E. Poeltl, J. K. McVey, *J. Chem. Phys.* **1984**, *80*, 1801–1811.
- [25] C. A. Southern, D. H. Levy, G. M. Florio, A. Longarte, T. S. Zwier, *J. Phys. Chem. A* **2003**, *107*, 4032–4040.
- [26] J. C. Baum, D. S. McClure, *J. Am. Chem. Soc.* **1980**, *102*, 720–727.
- [27] Y. Tomioka, H. Abe, N. Mikami, M. Ito, *J. Phys. Chem.* **1984**, *88*, 2263–2270.
- [28] C. K. Nandi, T. Chakraborty, *J. Chem. Phys.* **2004**, *120*, 8521–8527.
- [29] J. Antony, G. von Helden, G. Meijer, B. Schmidt, *J. Chem. Phys.* **2005**, *123*, 014305-1–014305-11.
- [30] G. M. Florio, E. L. Sibert III, T. S. Zwier, *Faraday Discuss.* **2001**, *118*, 315–330.
- [31] G. M. Florio, T. S. Zwier, E. M. Myshakin, K. D. Jordan, E. L. Sibert III, *J. Chem. Phys.* **2003**, *118*, 1735–1746.
- [32] J. M. Bakker, L. M. Aleese, G. von Helden, G. Meijer, *J. Chem. Phys.* **2003**, *119*, 11180–11185.
- [33] M. Schmitt, J. Küpper, D. Spangenberg, A. Westphal, *Chem. Phys.* **2000**, *254*, 349–361.
- [34] S. Gerstenkorn, P. Luc, *Atlas du Spectre d'Absorption de la Molécule d'Iode*, Laboratoire Aimé-Cotton CNRS II, Paris, **1982**.
- [35] R. Ahlrichs, M. Bär, M. Häser, H. Horn, C. Kölmel, *Chem. Phys. Lett.* **1989**, *162*, 165–169.
- [36] A. Schäfer, C. Huber, R. Ahlrichs, *J. Chem. Phys.* **1994**, *100*, 5829–5835.
- [37] C. Hättig, A. Köhn, *J. Chem. Phys.* **2002**, *117*, 6939–6951.
- [38] C. Hättig, *J. Chem. Phys.* **2002**, *117*, 7751–7761.
- [39] S. Grimme, M. Waletzke, *J. Chem. Phys.* **1999**, *111*, 5645–5655.
- [40] A. D. Becke, *J. Chem. Phys.* **1993**, *98*, 1372.
- [41] C. Lee, W. Yang, R. Parr, *Phys. Rev. B* **1988**, *37*, 785–789.
- [42] C. Peng, H. B. Schlegel, *Israel J. Chem.* **1994**, *33*, 449.
- [43] M. J. Frisch, G. W. Trucks, H. B. Schlegel, G. E. Scuseria, M. A. Robb, J. R. Cheeseman, J. A. Montgomery, Jr., T. Vreven, K. N. Kudin, J. C. Burant, J. M. Millam, S. S. Iyengar, J. Tomasi, V. Barone, B. Mennucci, M. Cossi, G. Scalmani, N. Rega, G. A. Petersson, H. Nakatsuji, M. Hada, M. Ehara, K. Toyota, R. Fukuda, J. Hasegawa, M. Ishida, T. Nakajima, Y. Honda, O. Kitao, H. Nakai, M. Klene, X. Li, J. E. Knox, H. P. Hratchian, J. B. Cross, C.

- Adamo, J. Jaramillo, R. Gomperts, R. E. Stratmann, O. Yazyev, A. J. Austin, R. Cammi, C. Pomelli, J. W. Ochterski, P. Y. Ayala, K. Morokuma, G. A. Voth, P. Salvador, J. J. Dannenberg, V. G. Zakrzewski, S. Dapprich, A. D. Daniels, M. C. Strain, O. Farkas, D. K. Malick, A. D. Rabuck, K. Raghavachari, J. B. Foresman, J. V. Ortiz, Q. Cui, A. G. Baboul, S. Clifford, J. Cio-slawski, B. B. Stefanov, G. Liu, A. Liashenko, P. Piskorz, I. Komaromi, R. L. Martin, D. J. Fox, T. Keith, M. A. Al-Laham, C. Y. Peng, A. Nanayakkara, M. Challacombe, P. M. W. Gill, B. Johnson, W. Chen, M. W. Wong, C. Gonzalez, J. A. Pople, *Gaussian03 (Revision a.1)*, Gaussian, Inc., Pittsburgh, PA, **2003**.
- [44] T. Helgaker, *Chem. Phys. Lett.* **1991**, *182*, 503–510.
- [45] A. Ostermeier, A. Gawelcyk, N. Hansen in *Parallel Problem Solving from Nature—PPSN III* (Eds.: Y. Davidor, H.-P. Schwefel, R. Männer), Springer, Berlin/Heidelberg, **1994**.
- [46] O. M. Shir, T. Bäck, *The Second Harmonic Generation Case Study as a Gateway for ES to Quantum Control Problems*, Proceedings of the Genetic and Evolutionary Computation Conference, ACM Press, London, UK, **2007**.
- [47] J. A. Hageman, R. Wehrens, R. de Gelder, W. L. Meerts, L. M. C. Buydens, *J. Chem. Phys.* **2000**, *113*, 7955–7962.
- [48] W. L. Meerts, M. Schmitt, G. Groenenboom, *Can. J. Chem.* **2004**, *82*, 804–819.
- [49] O. M. Shir, C. Siedschlag, T. Bäck, M. J. J. Vrakking, *Opt. Commun.* **2006**, *264*, 511–518.
- [50] L. L. Connell, S. M. Ohline, P. W. Joireman, T. C. Corcoran, P. M. Felker, *J. Chem. Phys.* **1992**, *96*, 2585–2593.
- [51] M. Onda, M. Asai, K. Takise, K. Kuwae, K. Hayami, A. Kuroe, M. Mori, H. Miyazaki, N. Suzuki, I. Yamaguchi, *J. Mol. Struct.* **1999**, *482*, 301–303.
- [52] J. Bicerano, H. F. Schaefer III, W. H. Miller, *J. Am. Chem. Soc.* **1983**, *105*, 2550–2553.
- [53] G. Bruno and L. Randaccio, *Acta Crystallogr. B* **1980**, *36*, 1711–1712.

Received: April 9, 2008

Revised: May 13, 2008

Published online on July 28, 2008